

1 **The impact of resolving the Rossby radius at mid-latitudes**
2 **in the ocean: results from a high-resolution version of the**
3 **Met Office GC2 coupled model**

4 **Helene T. Hewitt¹, Malcolm J. Roberts¹, Pat Hyder¹, Tim Graham¹, Jamie Rae¹,**
5 **Stephen E. Belcher¹, Romain Bourdallé-Badie⁴, Dan Copey¹, Andrew Coward²,**
6 **Catherine Guiavarch¹, Chris Harris¹, Richard Hill¹, Joël J.-M. Hirschi², Gurvan**
7 **Madec^{2,3}, Matthew S. Mizielski¹, Erica Neininger¹, Adrian L. New², Jean-**
8 **Christophe Rioual¹, Bablu Sinha², David Storkey¹, Ann Shelly¹, Livia Thorpe¹,**
9 **and Richard A. Wood¹**

10 [1]{Met Office, Exeter, United Kingdom}

11 [2]{National Oceanography Centre, Southampton, United Kingdom}

12 [3]{IPSL, Paris, France}

13 [4]{Mercator Océan, Toulouse, France}

14 Correspondence to: H. T. Hewitt (helene.hewitt@metoffice.gov.uk)

15

16 **Abstract**

17 There is mounting evidence that resolving mesoscale eddies and western boundary currents as
18 well as topographically-controlled flows can play an important role in air-sea interaction
19 associated with vertical and lateral transports of heat and salt. Here we describe the
20 development of the Met Office Global Coupled Model version 2 (GC2) with increased
21 resolution relative to the standard model: the ocean resolution is increased from $1/4^\circ$ to $1/12^\circ$
22 (28km to 9km at the Equator), the atmosphere resolution increased from 60km (N216) to
23 25km (N512) and the coupling period reduced from 3-hourly to hourly. The technical
24 developments that were required to build a version of the model at higher resolution are
25 described as well as results from a 20 year simulation. The results demonstrate the key role
26 played by the enhanced resolution of the ocean model: reduced Sea Surface Temperature
27 biases, improved ocean heat transports, deeper and stronger overturning circulation and a
28 stronger Antarctic Circumpolar Current. Our results suggest that the improvements seen here

1 require high resolution in both atmosphere and ocean components as well as high frequency
2 coupling. These results add to the body of evidence suggesting that ocean resolution is an
3 important consideration when developing coupled models for weather and climate
4 applications.

5

6 **1 Introduction**

7 On the scale of the Rossby radius, the ocean is rich with mesoscale eddies (Chelton et al.,
8 2011) and oceanic fronts. There is mounting evidence from satellite observations that
9 mesoscale features in the Sea Surface Temperature (SST) field can drive comparable
10 variations in atmospheric winds and surface fluxes (Chelton and Xie, 2010; Frenger et al.,
11 2015). While at the basin scale, observed correlations between SST and surface winds are
12 negatively correlated, indicating that the atmosphere is driving the ocean, in frontal regions
13 with high mesoscale activity, such as those associated with Western boundary currents, SST
14 and surface winds are positively correlated, implying that the ocean is driving the atmosphere
15 (Bryan et al., 2010). While the primary response to SST takes place in the atmospheric
16 boundary layer (Chelton and Xie, 2010), there is also evidence that divergence of surface
17 winds may give rise to vertical motions which may penetrate high into the troposphere
18 affecting storm tracks and clouds (e.g., Minobe et al., 2008; Sheldon and Czaja, 2014). Of
19 particular note is the intense rain band in the North Atlantic that follows the path of the Gulf
20 Stream/North Atlantic Current.

21 The recent CMIP5 ocean models have a horizontal resolution of between 1° and $1/4^\circ$.
22 However, with a resolution of 28km at the Equator down to 6km in the Canadian archipelago
23 (due to the tripolar grid), even $1/4^\circ$ remains insufficient to resolve mesoscale eddies which
24 have a typical scale of 50km in the deep ocean at mid-latitudes (Hallberg, 2013). Several
25 climate modelling groups have now built global coupled models with an “eddy resolving”
26 component (e.g., McClean et al., 2011; Bryan et al., 2010; Delworth et al., 2012; Small et al.,
27 2014; Griffies et al., 2015). In this paper, we describe results from coupling the $1/12^\circ$ ocean
28 model (ORCA12) produced by the Drakkar group (Marzocchi et al., 2015; Deshayes et al.,
29 2013; Treguier et al., 2012) to a 25 km (N512) resolution version of the Met Office Unified
30 Model (MetUM) atmosphere. This is the first version of the HadGEM3/GC series (Hewitt et
31 al., 2011; Williams et al., 2015) to resolve the Rossby radius in the ocean at mid-latitudes
32 (with a resolution of 9km at the Equator down to 2km in the Canadian archipelago) and the

1 first coupled experiment with the NEMO ORCA12 ocean configuration. The development of
2 a global coupled model with atmosphere and ocean components of this resolution as well as
3 hourly coupling is the current state of the art for global climate modelling.

4 Evidence from forced ocean simulations demonstrates that resolution enables a more realistic
5 representation of both eddy kinetic energy (Hurlburt et al., 2009; Griffies et al., 2015), narrow
6 boundary currents (e.g., Marzocchi et al., 2015) and representation of complex topography, in
7 particular the sills which connect ocean basins (e.g., improved overflows in the VIKING
8 model at $1/20^\circ$ resolution; Behrens, 2013). In this paper we investigate how ocean resolution
9 drives large-scale changes not only in the ocean but also in the climate system. Changes in the
10 ocean circulation could be important both for present and future climate; for example, in an
11 ocean-only model with a simple domain, Zhang and Vallis (2013) have shown that the
12 changes in mean circulation due to eddy-resolving resolution can affect the net ocean heat
13 uptake under global warming scenarios.

14 In this paper, the model is described in section 2. Our results (section 3) describe the relative
15 impact of the three changes to the model; ocean resolution, atmosphere resolution and
16 coupling frequency. Finally in section 4 we summarise and discuss the results.

17

18 **2 Model description**

19 The development of the high resolution coupled climate model is based on the Met Office
20 Global Coupled model version 2 (GC2; Williams et al., 2015). GC2 is comprised of the Met
21 Office Unified Model (MetUM; GA6) atmosphere, the JULES land surface model (Best et al.,
22 2011; GL6), the NEMO ocean model (Madec, 2014; GO5; Megann et al., 2014) and the Los
23 Alamos CICE sea-ice model (Hunke et al., 2010; GSI6; Rae et al., 2015). The standard
24 configuration for GC2 has a 60km resolution atmosphere coupled to $1/4^\circ$ (28km at the
25 Equator reducing polewards) ocean (N216-ORCA025) with coupling between the
26 components (as described in Hewitt et al., 2011) every three hours. GA6 has 85 vertical levels
27 while GO5 has 75 vertical levels with 1m resolution in the top 10m of the ocean (Megann et
28 al., 2014). Although vertical resolution is not explored here, we include details of the vertical
29 levels in appendix A.

1 In addition to GC2, this paper describes three modified versions of GC2 with increased
2 atmosphere resolution, increased coupling frequency and increased ocean resolution. The
3 different model experiments are described below and summarised in Table 1.

4 GC2 has been run with a high 25km (N512) atmosphere resolution and the standard
5 (ORCA025) resolution ocean and we will refer to this as GC2-N512. The scientific
6 differences between N216 and N512 are minimal, as described in Walters et al. (in prep), and
7 are principally associated with the time step (modified from 15min to 10min) and the
8 resolution of the external boundary conditions such as the orography.

9 To facilitate direct scientific comparison with the 1/12° ORCA12 (9km at the Equator
10 reducing polewards) configuration of NEMO, which was developed using NEMO v3.5 rather
11 than 3.4 (Marzocchi et al., 2015), a modified configuration of GC2, referred to here for
12 convenience as GC2.1 was developed. The key scientific and technical changes made to
13 GC2.1 are:

- 14 • a reduction in the coupling period from 3-hourly to hourly
- 15 • an upgrade to the non-linear free surface scheme rather than the linear free surface
- 16 • a small reduction in the ocean timestep from 1350s to 1200s (to accommodate hourly
17 coupling)
- 18 • small changes associated with river outflows; outflows prescribed over 15m rather
19 than 10m with an enhanced vertical mixing in the outflow region of $1 \times 10^{-3} \text{m}^2 \text{s}^{-1}$ rather
20 than $2 \times 10^{-3} \text{m}^2 \text{s}^{-1}$
- 21 • an upgrade of the sea ice model from CICE4 to CICE5 (Hunke et al., 2015). This
22 upgrade was for technical reasons and the science of the sea ice configuration remains
23 unchanged.

24 The reduction of the coupling period in GC2.1 did not lead to coupled ocean/sea ice
25 instabilities as described by Hallberg (2014).

26 To assess the impact of ocean resolution, a traceable GC2.1 configuration with ORCA12 was
27 then built (further technical details and model performance issues are discussed in appendix
28 B). We chose to increase the atmosphere resolution to N512 in order to maintain a similar
29 ratio of atmosphere to ocean grids. We will refer to this configuration as GC2.1-N512O12
30 (i.e., increased atmosphere and ocean resolution).

31

1 The differences between ORCA025 and ORCA12 in GC2.1 are:

- 2 • a reduction in the time step from 1200s to 240s
- 3 • a reduction in the isoneutral tracer diffusion from $300 \text{ m}^2\text{s}^{-1}$ to $125 \text{ m}^2\text{s}^{-1}$
- 4 • a reduction in the bilaplacian viscosity from $1.5 \times 10^{11} \text{ m}^2\text{s}^{-1}$ to $1.25 \times 10^{10} \text{ m}^2\text{s}^{-1}$

5 We note here that the parameter settings in GC2.1-N512O12 have not been tuned for the
6 coupled model; the model was run using the majority of parameter settings from the forced
7 ocean-only ORCA12 runs of Marzocchi et al. (2015). While reducing the isoneutral tracer
8 diffusivity is consistent with the increase in resolution, we note that results may have some
9 sensitivity to its magnitude. Experiments to investigate the impact of this parameter in GC2
10 were not performed but will be pursued in future work with GC3 (the next version of the
11 coupled model).

12 GC2.1-N512O12 was found to be very sensitive to features that had not proved to be a
13 problem in previous ocean-only integrations (e.g., Marzocchi et al., 2015). For example, the
14 model became unstable on the east coast of the UK every 6-12 months of simulation due to
15 extreme values in the velocity field, likely due to the lack of tidal dissipation in the model
16 which is very important in this region. The model was restarted from these failures with a
17 small random perturbation to the atmosphere temperature field in a similar way to treatment
18 of “grid-point instabilities” previously seen in atmosphere models (e.g., Mizielinski et al
19 2014). The underlying problem with this unstable ocean point will be addressed in future
20 developments of the ORCA12 configuration.

21 The GC2 and GC2.1 experiments were run for 20 years with fixed atmospheric radiative
22 forcing representative of the present day (with greenhouse gas and aerosol values for the year
23 2000). All experiments were initialised in the following way:

- 24 • atmosphere: N216 and N512 both from September year 18 of the model state of a
25 previous N512 GA6 (Walters et al., in prep) forced atmosphere integration with
26 forcing representative of the year 2000, so that the land surface properties are at quasi-
27 equilibrium;
- 28 • ocean: temperature and salinity from the EN3 observational dataset (Ingleby and
29 Huddleston, 2007) 2004-8 September average with velocities initialised to zero;
- 30 • sea ice: 20 year September mean from a HadGEM1 (Johns et al., 2006) experiment
31 representative of a period centred on 1978.

- These latter two are the standard method for initialisation of “present day” coupled simulations at the Met Office.

The choice of the most appropriate ratio between ocean and atmosphere resolution remains an open research question worthy of further study. Short (two year) integrations using both higher and lower atmosphere resolutions coupled to ORCA12 were completed, although due to the short length of the integrations, they are not analysed here. In particular, a configuration using an N768 (17km) atmosphere led to a marked increase in the frequency of the type of model instabilities described earlier (from 1-2 per year to 5-6 per year).

3 Impact of model resolution on surface properties, heat transport and ocean circulation

The results shown in this section derive from 20 year simulations of the four experiments described in table 1, initialised and forced in an identical way.

a. Surface Properties

The pattern of large-scale biases in SST fields in Hadley Centre coupled climate models have remained largely unchanged since the models first ran without flux correction (e.g., Gordon et al., 2000); the large-scale biases exhibit warming in the Southern Ocean, cooling in the North Pacific and North Atlantic and warming in upwelling/stratocumulus regions off the western coasts of South America and Africa. Many of these biases are also very common in other models (e.g. Small et al., 2014). In contrast to the pattern, the magnitude of the SST biases has changed between model versions; in particular, comparing GC2 and HadGEM2-AO (Figure 1 of Williams et al., 2015), shows that the magnitude of the Northern hemisphere cooling was reduced in GC2 while the magnitude of the Southern Ocean warming was increased.

The time-series of the global mean Top of Atmosphere (TOA) radiation imbalance in the four models (Figure 1a) shows that the experiments with high (N512) atmosphere resolution have TOAs that are generally higher at the start of the experiments. However after 20 years all the experiments are starting to converge to a similar net TOA, as the shortwave and long-wave components adjust. Although the TOA-SST relationship is poorly defined (since the TOA imbalance is related to the rate of change of net ocean heat content; Palmer and McNeill,

1 2014), the integrated effect of the higher net TOA in the N512 experiments can be seen in the
2 timeseries of the global mean SST (Figure 1b) with GC2-N512 and GC2.1-N512O12 having
3 higher global mean SSTs.

4 In spite of the differences in global mean SST, major changes to the pattern and magnitude of
5 SST biases are only seen with both high atmosphere and ocean resolution (Figure 2). In
6 GC2.1-N512O12, the large-scale underlying SST biases are reduced relative to GC2 and
7 GC2.1 (Figure 3): the warm bias in the Southern Ocean; cold bias in North Atlantic and North
8 Pacific and warm biases in stratocumulus regions. Similar reductions in SST biases with high
9 atmosphere and ocean resolution were also seen in Small et al. (2015). The increase in ocean
10 resolution is key to this improvement: when only atmosphere resolution is increased (compare
11 Figures 2a and b), there is only a small reduction in the warm bias associated with
12 stratocumulus regions (west of South America and Africa), while increased coupling
13 frequency (compare Figures 2a and c) shows only minor changes in SST biases.

14 In GC2 there is a cold bias in the North Atlantic subpolar gyre (SPG), Greenland-Iceland-
15 Norwegian (GIN) Seas and the Arctic. GC2.1-N512O12 shows a warming of several degrees
16 in the SPG and GIN seas relative to GC2 (see reduced cold bias in Figure 2d) and a very large
17 warming in the Central Arctic. The warming in the Central Arctic is associated with a
18 warming in the subpolar gyre, enhanced northward heat transport into the Arctic and melting
19 back of the sea ice edge in the Arctic (see below).

20 Resolution appears to have less of an impact on Sea Surface Salinity (SSS; Figure 4).
21 Nevertheless, there are reductions in high salinity biases in the Indian Ocean and the Pacific
22 (in particular, in the salinity maximum in the subtropical gyre of the South Pacific) as well as
23 reductions in the Arctic biases (although these are very sensitive to the distribution of sea ice).

24

25 *b. Sea ice*

26 The changes to the SST also affect sea ice distribution in both hemispheres. The seasonal
27 cycle of ice extent in the Arctic (Figure 5a) shows that the warm SSTs in GC2.1-N512O12 at
28 high Northern latitudes reduce the ice extent throughout the year. The March ice
29 concentrations in the Arctic (Figure 6) clearly demonstrate that the impact on the sea ice is
30 concentrated in the GIN seas with the sea ice edge in GC2.1-N512O12 much further north
31 than seen in GC2 with the edge being north of Spitzbergen and into the Barents Sea.

1 In comparison, the reduction in the warm bias in the Southern hemisphere leads to only
2 modest increases in the total sea ice extent (Figure 5b); the overall warming bias associated
3 with the lack of super-cooled liquid clouds (Bodas-Salcedo et al., 2014; Bodas-Salcedo et al.,
4 in press) still dominates the melting of sea ice. The small increase in sea ice extent is very
5 inhomogeneous; indeed, some regions in the Southern Ocean such as the Weddell Sea
6 actually show reductions in sea ice extent in GC2.1-N512O12 (Figure 6). The reduction in the
7 Weddell Sea is associated with the formation of polynyas in that region (see below).

8

9 *c. Sub-surface ocean drifts*

10 Conservation of heat within the climate system implies that the net heat uptake by the ocean
11 should nearly balance the net radiative imbalance at the TOA. GC2.1-N512O12 has the
12 highest TOA imbalance of the four models (Table 2) and therefore will have the greatest net
13 heat uptake. Both models with increased atmosphere resolution (GC2-N512 and GC2.1-
14 N512O12) have a higher TOA imbalance than the models with lower atmosphere resolution
15 (GC2 and GC2.1).

16 The global temperature profiles (Figure 7a) show that GC2-N512 and GC2.1-N512O12 do
17 indeed have greater increases in temperature as a function of depth than either of the low
18 resolution models (GC2 and GC2.1), which is consistent with the higher TOA imbalance. The
19 main difference between GC2-N512 and GC2.1-N512O12 is that the increase in heat uptake
20 extends deeper in GC2.1-N512O12. This difference is also apparent in the global mean SST
21 anomaly (Table 2); the SST anomaly for years 11-20 in GC2.1-N512O12 is 0.44 K compared
22 with 0.60 K in GC2-N512, while the TOA imbalance is 2.02 W/m² and 1.79 W/m²
23 respectively. This shows that the ORCA12 version of the model is able to transport heat to
24 depth more effectively.

25 An increase in heat uptake in GC2.1-N512O12 relative to GC2-N512 is unexpected when
26 considering the results of Griffies et al. (2015). Griffies et al. (2015) show that an increase in
27 eddy activity produces upward eddy transport with a net effect of reduced heat uptake. Our
28 results do not show a similar result suggesting that either the mean circulation is more
29 effectively transporting heat downwards (which is consistent with an increased overturning
30 circulation) or perhaps that there is an increase in spurious diapycnal mixing. Producing a
31 budget analysis in the future would help to address this issue.

1 The distribution of the subsurface temperature changes varies depending on the latitudinal
2 range. South of 30°S (Figure 7b), near surface warming is reduced in GC2.1-N512O12
3 relative to the other models. In the Tropics (30°S-30°N; Figure 7c), GC2.1-N512O12 shows
4 increased warming shallower than 500m relative to the low resolution models but reduced
5 relative to GC2-N512. The Tropics also show increased warming at depth in GC2.1-
6 N512O12. The largest increase in near surface temperatures in GC2.1-N512O12 relative to
7 the other models occurs north of 30°N (Figure 7d) with the surface warming displacing a cold
8 bias to deeper in the water column. The warming is particularly concentrated north of 65°N
9 (Figure 7e) where it has previously been shown that Arctic sea ice melts back.

10 Drifts in sub-surface salinity show that GC2.1-N512O12 generally has larger salinity drifts
11 between 500 and 1000m (Figure 8a) which is largely associated with the region south of 30°S
12 (Figure 8b). In the northern hemisphere, drifts in salinity between 1000 and 2000m are also
13 more pronounced in GC2.1-N512O12 than the other models (Figure 8d). In contrast, large
14 fresh biases north of 65°N in most of the models is much reduced in GC2.1-N512O12 (Figure
15 8e). Understanding salinity drifts and their relationship to freshwater forcing is complex (eg,
16 Pardaens et al. 2003) and this aspect of the model performance will require further
17 investigation.

18

19 *d. Mixed layer depths*

20 In general over the open oceans, the mixed layer depths¹ (Figure 6) are very similar across the
21 different models and it is in the deep water formation regions where we see inter-hemispheric
22 changes. Winter mixed layers in the Northern hemispheres in GC2.1-N512O12 show a
23 reduction in the North Atlantic subpolar gyre. Most notably, in GC2.1-N512O12 deep mixed
24 layers are less extensive south of Greenland than in GC2 and are confined to the centre of the
25 Labrador Sea. Similar changes in Labrador Sea deep convection have been seen in sensitivity
26 experiments when overflow properties are improved (Graham et al., in prep.). The deeper
27 mixed layers in the Arctic in GC2.1-N512O12 are consistent with warmer SSTs and reduced
28 sea ice extent in that region exposing open water.

¹ Mixed layer depth is calculated as the depth at which density changes by 0.01 kg m⁻³ relative to the density at 10m

1 The similarity of the mixed layer depths across the Southern Ocean demonstrate that it is not
2 changes to the mixed layer depths that lead to a reduction in the Southern Ocean warm bias.
3 As mentioned in the previous section, in the Weddell Sea, GC2.1-N512O12 has very deep
4 mixed layers (maximum of 800m in the decadal mean) linked to the formation of polynyas.
5 Polynya formation varies both spatially and on an interannual basis over the last 9 years of the
6 simulation (Figure 9); the polynya first appears in year 12 and persists for 5 years before
7 disappearing, starting to re-emerge in year 18 and reaching a depth of 2070m in year 20. The
8 appearance of the polynya in this decade explains the lack of increase of sea ice extent in that
9 region (as seen in Figure 6). Deeper winter mixed layers in GC2.1-N512O12 are also evident
10 through the mid-latitudes in the formation zones for Sub-Antarctic Mode Waters and
11 Antarctic Intermediate Waters. These could be due to the reduced warm bias (cooler SSTs) in
12 these regions (Figure 2).

13

14 *e. Ocean Circulation*

15 The improvements seen in the large-scale SST biases with high atmosphere and ocean
16 resolution (Figure 3) represent an overall improvement in the model simulation with warming
17 in the Northern hemisphere and cooling in the Southern hemisphere. This pattern is
18 reminiscent of inter-hemispheric modes that occur as a result of changes in the large-scale
19 thermohaline circulation (Vellinga and Wu, 2004). The meridional overturning at 24°N in our
20 simulations increases by O(1.5 Sv) in GC2.1 and in GC2.1-N512O12 by a further O(1.5 Sv)
21 (Table 2). At 30°S, a change of O(3 Sv) is only seen in GC2.1-N512O12. The enhanced
22 meridional overturning is therefore attributed to the increased ocean resolution in combination
23 with the increased coupling frequency. The changes in the meridional overturning circulation
24 (Figure 10) are dominated by changes in the cell associated with North Atlantic Deep Water
25 (NADW) with changes extending into the Southern hemisphere. Examination of the
26 overturning in density space would further support this analysis but this was not possible with
27 the diagnostics available from this simulation and will be addressed in future simulations.

28 At the northern end of the NADW cell, we see increases in the volume flux of dense
29 overflows between the GIN Seas and the Atlantic (Table 2) that are consistent with the
30 NADW cell being strengthened both by the GIN sea sources and better representation of sills.
31 The volume flux of overflow waters across Denmark Straits generally reduces fairly rapidly
32 in ORCA025 runs (Figure 11a) but in GC2.1-N512O12 the overflow remains closer to the

1 observed value of 2.9 - 3.7 Sv (Dickson and Brown, 1994; Macrander et al., 2005; Jochumsen
 2 et al., 2012). This appears to also contribute to a deeper (as well as stronger) NADW outflow
 3 in GC2-N512O12 (Figure 10) and we suggest that this is likely to be associated with the
 4 increased resolution of the topography in the region of the overflows.

5 The Antarctic Circumpolar Current (ACC) usually drifts in the ORCA025 GC models from
 6 an initial value of approximately 150 Sv to below 100 Sv (Figure 11b). Increased ocean
 7 resolution counteracts that, with the ACC stabilising close to 130 Sv in GC2-N512O12. This
 8 value is close to the observations which suggest an ACC transport of 137 ± 8 Sv
 9 (Cunningham et al., 2003; Meredith et al., 2011). The increase in the transport in the ACC can
 10 be explained by changes in the density field; the meridional density gradients across the ACC
 11 (not shown) are increased in GC2.1-N512O12 (with steeper isopycnals) than in GC2. This
 12 result is consistent with increased southward flow, and stronger upwelling, of NADW to the
 13 north of the ACC (Allison et al., 2011) and increased convection to the south of the ACC in
 14 the Weddell Sea (Hirabara et al., 2012). The Southern Ocean winds (not shown) respond
 15 differently across the four simulations (including a small increase in GC2.1-N512O12 and a
 16 decrease in GC2.1). Jones et al. (2011) have shown that the transient response of the ACC to
 17 changes in winds can be seen within 10 years, suggesting that it is not surprising that we are
 18 able to detect changes in the ACC in this set of experiments.

19

20 *f. Heat transport*

21 As described in Gordon et al. (2000), drifts in volume averaged ocean temperature can be
 22 related to discrepancies between the actual heat transports by the ocean and the heat transport
 23 implied by the surface fluxes, i.e.

$$24 \quad \frac{\partial \rho c_p \langle \theta \rangle}{\partial t} + \oint \rho c_p (\bar{v}\bar{\theta} + \overline{v'\theta'}) dS + \oint \rho c_p A_{iso} \nabla_{\rho} \theta dS = \int F dA, \quad (1)$$

25 where $\langle \theta \rangle$ is the volume integrated temperature, $\bar{v}\bar{\theta}$ and $\overline{v'\theta'}$ are the time mean and time
 26 varying components of the ocean meridional heat transports, ρc_p is density multiplied by
 27 specific heat capacity, A_{iso} is the isoneutral diffusivity, $\nabla_{\rho} \theta$ is the isoneutral gradients of
 28 temperature, F is the surface heat flux, $dS (=dx*dz)$ is the cross sectional area (x and z denote
 29 the zonal and vertical directions) and dA is the surface area of the region. For our purposes
 30 here, we make the assumption that the isoneutral fluxes are generally smaller than the other
 31 terms (isoneutral diffusive fluxes are very small when integrated over full depth).

1 Figure 12a shows the global northward heat transport in all four simulations. There are some
 2 changes in the northern hemisphere in the GC2.1 simulation with the change to hourly
 3 coupling, while changes in the southern hemisphere are only seen in GC2.1-N512O12
 4 suggesting that these changes are driven by the increase in ocean resolution. The reduction in
 5 southward heat transport in GC2.1-N512O12 centred at 45°S is highly unusual; although the
 6 change does not lie outside interannual variability, a change of this magnitude in the multi-
 7 year mean heat transport has not been seen in any other development runs of the GC series.
 8 The modelled changes in the heat transports suggest that ocean processes are important in this
 9 region, which is particularly relevant given the uncertainty in surface heat fluxes in the
 10 Southern Ocean (Cerovecki et al., 2011). The increase in total heat transport comes primarily
 11 from the time mean heat transport (not shown). This suggests that increased resolution has
 12 either changed the mean circulation or the temperature profile. In contrast, if the increased
 13 heat transport was due to the time varying heat transport, this would imply a direct role for
 14 mesoscale eddies. As seen in previous sections, GC2.1-N512O12 shows changes in both the
 15 circulation and the temperature profiles. The decreased southward heat transport in the
 16 Southern Ocean of GC2.1-N512O12 could – at least partly - explain the reduced warm bias.

17 By comparing actual ocean heat transports with those implied by surface fluxes (i.e., the
 18 second term of the left-hand side of Eqn. 1 with the right-hand side of Eqn. 1), this gives an
 19 indication of the volume averaged drift in temperature (first term on the left-hand side of Eqn.
 20 1). To remove the effect of the net radiative imbalance, the implied ocean heat transport is
 21 calculated by subtracting the globally averaged imbalance from the surface fluxes before
 22 integrating zonally and meridionally. This is equivalent to removing a globally integrated
 23 temperature drift from the left-hand side of Eqn. 1. This can be described as:

$$24 \quad \frac{\partial \rho c_p \langle \theta \rangle - \bar{\theta}}{\partial t} + \oint \rho c_p (\bar{v}\bar{\theta} + \overline{v'\theta'}) dS = \int (F - \bar{F}) dA, \quad (2)$$

25 where $\bar{\theta}$ and \bar{F} are the global mean temperature and surface flux respectively. Eqn. 2 shows
 26 that a residual imbalance between the implied and actual ocean heat transports is indicative of
 27 local temperature drifts. Both globally and in the Atlantic basin (Figure 12a,b) GC2.1-
 28 N512O12 can be seen to be as close to local balance as any of the other models, suggesting
 29 that the net drifts will be of a similar magnitude (in agreement with Figure 5).

30 Ocean resolution is the driving factor in a 0.2PW increase in the northward heat transport in
 31 the Atlantic; the modelled heat transports in GC2.1-N512O12 are generally within the error
 32 bars of the observations (Ganachaud and Wunsch, 2003; Figure 12b) in contrast to the other

1 models with the lower resolution ocean component. The change in heat transport is linked to
2 an increase in the overturning circulation (previous section), which is unsurprising given the
3 dominant role of the meridional overturning circulation in the Atlantic heat transport (Hall
4 and Bryden, 1982).

5

6 **4 Summary and Discussion**

7 In this paper we have shown results from a coupled climate model with an eddy resolving
8 ($1/12^\circ$) ocean component coupled to a high resolution (25 km) atmosphere component. When
9 the SST bias from this climate simulation is compared to that from the Met Office standard
10 resolution climate model, with eddy permitting ($1/4^\circ$) ocean component and 60km atmosphere
11 component, it is apparent that major SST biases in the Southern Ocean and North Atlantic and
12 North Pacific have been reduced. Comparable experiments increasing only the atmosphere
13 resolution or the coupling frequency, demonstrate that increased ocean resolution is the key
14 driver for this change.

15 At the enhanced ocean resolution, the ocean circulation leads to increased poleward ocean
16 heat transport in the Northern hemisphere and reduced poleward ocean heat transport in the
17 Southern hemisphere. The change in the northward heat transport is driven at least in part by
18 an enhanced NADW cell. The stronger ACC at high resolution may be associated with a
19 number of factors: enhanced windstresses, increased deep water formation in the Weddell Sea
20 due to the presence of a polynya, enhanced southward transport of NADW and eddy fluxes.
21 Changes in the global heat transports produce a shift in the large-scale biases, cooling the
22 Southern Ocean and warming the North Atlantic and North Pacific. We have shown that heat
23 penetrates deeper in our $1/12^\circ$ model; Griffies et al. (2015) have demonstrated that mesoscale
24 eddies transport heat upwards so it is likely that the increased transport of heat to depth is
25 achieved by the time-mean as seen in transient experiments such as Banks and Gregory
26 (2006). Future work will be focused on understanding the relative roles of resolving overflow
27 topography (Behrens, 2013), eddy processes within the ocean including compensation and
28 saturation (e.g., Munday et al., 2013) and air-sea interaction on the eddy scale (Roberts et al.,
29 in prep.) in driving the large-scale changes.

30 Relative to the recent high resolution results of Small et al. (2014) and Griffies et al. (2015),
31 our results emphasise the importance of increasing both ocean resolution and coupling
32 frequency. Griffies et al. (2015) show smaller reductions in SST biases than seen here when

1 moving from $1/4^\circ$ to $1/10^\circ$ resolution presumably related to keeping the atmosphere resolution
2 unchanged. Enhanced coupling frequency along with enhanced vertical resolution near the
3 air-sea interface both in the ocean (Megann et al., 2014) and atmosphere (Walters et al., in
4 prep) is one feature of our model setup that is missing in Small et al. (2014). These aspects of
5 the model setup may be especially important in regions of strong air-sea interaction including
6 the stratocumulus regions where we see large improvements in the GC2.1-N512O12
7 simulation. Further work is required to quantify whether high resolution in the atmosphere
8 component is necessary in combination with the high resolution ocean components and high
9 frequency coupling to produce the results described in this paper.

10 As described in section 2, one of the changes to the ocean model at higher resolution was a
11 reduction in the isoneutral diffusivity. Pradal and Gnanadesikan (2014) show that a reduction
12 in the isoneutral diffusivity from $800 \text{ m}^2\text{s}^{-1}$ to $400 \text{ m}^2\text{s}^{-1}$ in a coarse resolution climate model
13 is associated with cooling of order 1°C at high latitudes after 500 years. Given that the results
14 here exhibit some consistency with those of Pradal and Gnanadesikan (2014) in the Southern
15 Ocean, further work is required to quantify the role of isoneutral diffusivity in producing
16 changes in SST on decadal timescales.

17 One caveat of these results is that the parallel simulations lasted only 20 years. However, the
18 broad similarity of the results presented here compared with those of Small et al. (2014) from
19 over 100 years of simulation suggest that the results are reasonably robust. In terms of model
20 drift, climate models typically have a fast adjustment within the first five years (Sanchez-
21 Gomez et al., 2016). Large adjustments over the first 20 years are generally followed by a
22 multi-centennial drift towards equilibrium between ocean properties and the net TOA flux
23 (Banks et al., 2007). Longer simulations and further analyses will enable the robustness of the
24 results presented here (including wind-SST feedbacks) to be more fully understood.

25 In the results presented here, the $1/12^\circ$ ocean model, which has a resolution of approximately
26 7 km at mid-latitudes, is coupled to an N512 atmosphere model, which has a resolution of 25
27 km. The relative importance of the atmosphere and ocean resolution remains a question which
28 will continue to be addressed in the community. We suggest that an atmosphere:ocean ratio of
29 4:1 may be too high for the atmosphere to fully respond to the details of the ocean mesoscale.
30 Future work will investigate the impact of coupling to even higher resolution atmosphere
31 models to investigate the role of the atmosphere:ocean ratio.

1 As we move towards using coupled models for prediction on timescales from days to
2 centuries, the results presented here are highly relevant to prediction up to decadal timescales
3 where data assimilation is employed. A coupled model that more faithfully produces the
4 current state of the ocean will rely less on data assimilation for correcting large-scale biases
5 and better represent spatial anomalies that control the large-scale variability. While there are
6 many regions where subsurface drifts are improved at ORCA12 resolution, reducing the drifts
7 seen in mid-depth salinity will be important.

8 The ocean data assimilation scheme used in Met Office systems is called NEMOVAR,
9 employed in a 3DVar first-guess-at-appropriate-time (FGAT) mode (Waters et al., 2015). A
10 new version of NEMOVAR has recently been developed (Weaver et al. 2016) which uses a
11 2D implicit diffusion operator to model the horizontal background error covariances, one of
12 the most computationally expensive aspects of the scheme. This new version has been
13 developed in such a way that the number of costly global communications are minimised and
14 is therefore expected to scale well with resolution. Preliminary implementations of this
15 scheme in the ORCA12 configuration indicate that it will be feasible to implement it for
16 operational ocean forecasting applications.

17 A key question for these timescales is whether employing enhanced resolution will address
18 the known problem of low signal-to-noise ratios (Eade et al., 2014) that has led to the need for
19 large ensembles for seasonal to decadal forecasting in lower resolution systems. Future work
20 to understand the drivers of large-scale bias reduction will support targeted experiments to
21 address the relative roles of resolution and ensemble size at these timescales. That said, ocean
22 resolution is clearly not going to solve all the issues in climate models; atmosphere errors
23 often dominate surface biases and, even at high resolution, ocean models need improved
24 representation of sub-gridscale processes.

25

26

27 **Code availability**

28 The MetUM is available for use under licence. A number of research organizations and
29 national meteorological services use the MetUM in collaboration with the Met Office to
30 undertake basic atmospheric process research, produce forecasts, develop the MetUM code
31 and build and evaluate Earth system models. For further information on how to apply for a
32 licence see <http://www.metoffice.gov.uk/research/collaboration/um-collaboration>. JULES is

1 available under licence free of charge. For further information on how to gain permission to
2 use JULES for research purposes see <https://jules.jchmr.org/software-and-documentation>. The
3 model code for NEMO v3.4 and v3.5 is available from the NEMO website ([www.nemo-](http://www.nemo-ocean.eu)
4 [ocean.eu](http://www.nemo-ocean.eu)). On registering, individuals can access the code using the open source subversion
5 software (<http://subversion.apache.org/>). The model code for CICE is freely available
6 (<http://oceans11.lanl.gov/trac/CICE/wiki/SourceCode>) from the United States Los Alamos
7 National Laboratory. In order to implement the scientific configuration of GC2/GC2.1 and to
8 allow the components to work together, a number of branches (code changes) are applied to
9 the above codes. Please contact the authors for more information on these branches and how
10 to obtain them.

11

12 **Appendix A: Model vertical levels**

13 The sensitivity to vertical resolution is not explored in this paper. However, a reduced
14 description of the vertical levels in GA6 (Table A1) and GO5 (Table A2) are included to
15 allow comparison with other models. For the full vertical levels, see Walters et al. (in prep.)
16 and Megann et al. (2014), respectively.

Level	Rho_height (m)
1	10.00
10	730.00
20	2796.67
30	6196.67
40	10930.12
50	17012.40
60	24710.70
70	35927.89
80	58978.35
85	82050.01

17 Table A1: Reduced list of level in GA6 which has 85 vertical levels

1

Level	Depth (m)	Thickness (m)
1	0.51	1.02
10	13.99	2.37
20	61.11	7.58
30	180.55	18.27
40	508.64	53.76
50	1387.38	125.29
60	2955.57	181.33
65	3897.98	194.29
70	4888.07	200.97
75	5902.06	204.23

2 Table A2: Reduced list of levels and layer thicknesses in GO5 which has 75 vertical levels

3

1 **Appendix B: Model performance and technical aspects**

2 The GC2.1 configuration was the first in which several further technical components of the
3 coupled system were considered essential to make the simulation manageable. The coupler
4 was upgraded from OASIS3 to OASIS3-MCT (Valcke et al, 2015) in order to improve
5 parallelisation of the coupling, particularly given the increased coupling frequency.

6 ORCA025 files are typically written as one file per processor by standard GC2 configurations
7 and combined into a single file prior to analysis as a post processing step. However, as HPC
8 parallel file systems are generally tuned for high bandwidth on large files and as GC2.1-
9 N512O12 configurations allocate 50 of the 80 nodes used by the full coupled system to the
10 ocean, this led to performance and functional issues when running on 1600 or more cores.
11 The NEMO XIOS diagnostic server (Madec, 2014) provides an asynchronous IO server
12 capability that allows the diagnostic files to be output as fewer larger files (although the
13 restart files are still written as one file per processor). Its introduction in the model allowed us
14 to overcome the limitations of the file system.

15 Land suppression was used for the NEMO and CICE models, so that processors are only
16 assigned to regions with active ocean points. This leads to a significant gain in core count,
17 although it meant that the automated large-scale diagnostics usually produced by NEMO
18 (zonal mean heat transports, meridional overturning) could not be generated.

19 Data volumes from this experiment were particularly large due to the output of additional
20 hourly and 3-hourly fluxes in order to examine the coupling processes in more detail. Each
21 month of model output comprised: ocean monthly mean files (netCDF) of 87GB together
22 with 6GB of daily files, sea-ice output (netCDF) of 57GB per month (with an additional
23 48GB of hourly output), and atmosphere output (PP format) of 100 GB per month. In total,
24 the 20 years of simulation produced 85 TB of data.

25 Little optimisation of the model was attempted since GC2.1 is not intended to be supported in
26 the long-term. Its successor, GC3, will be used for CMIP6. The GC2.1-N512O12 model used
27 80 full nodes (each of 32 cores) of an IBM Power 7 HPC, of which 55 were allocated to the
28 ocean/sea ice component (including 5 for the IO servers) and 25 for the atmosphere/land
29 component. The model throughput was 4 months per wall-clock day.

30 For previous model resolutions, the SCRIP utility (Jones, 1998) was used to generate the
31 conservative remapping files used to regrid coupling data between the ocean and atmosphere

1 grids (for temperature and fluxes), with bilinear interpolation used for the winds and surface
2 currents. However, due to the size of the high resolution grids used here, and the serial nature
3 of SCRIP, a different method was required. ESMF (ESMF, 2014; a package of parallelised
4 tools that use the same input grid descriptions as SCRIP, but can be run in parallel) was
5 therefore used to generate the remapping weights.

6

7

8 **Acknowledgements**

9 We thank the Editor and the two reviewers (Stephen Griffies and Andy Hogg) for their
10 constructive comments. Matt Martin provided useful input on data assimilation for ORCA12.
11 This work was primarily supported by the Joint DECC/Defra Met Office Hadley Centre
12 Climate Programme (GA01101). Part of the work was undertaken with National Capability
13 funding from NERC for ocean modelling. We acknowledge use of the MONSooN system, a
14 collaborative facility supplied under the Met Office-NERC Joint Weather and Climate
15 Research Programme (JWCRP). Met Office authors were supported by the joint UK
16 DECC/DEFRA Met Office Hadley Centre Climate Programme (GA01101). MR
17 acknowledges support from the EU FP7 IS-ENES2 project for work on ESMF and regriding
18 tools. We acknowledge the considerable effort on development and evaluation of ORCA12 by
19 the DRAKKAR community. HH thanks IH.

20

21

22 **References**

23 Allison, L. C., Johnson, H. L. and Marshall, D. P.: Spin-up and adjustment of the Antarctic
24 Circumpolar Current and global pycnocline, *J. Mar. Res.*, 69, 167-189, 2011.

25 Banks, H. T. and Gregory, J. M.: Mechanisms of ocean heat uptake in a coupled climate
26 model and the implications for tracer based predictions of ocean heat uptake, *Geophys. Res.*
27 *Let.*, 33, L076208, doi:10.1029/2005GL025352, 2006.

28 Banks, H. T., Stark, S. and Keen, A. B.: The adjustment of the coupled climate model
29 HadGEM1 towards equilibrium and the impact on global climate, *J. Climate*, 20, 5815-5826,
30 2007.

1 Behrens, E.: The oceanic response to Greenland melting: the effect of increasing model
2 resolution, PhD thesis, University of Kiel, 2013.

3 Best, M. J., Pryor, M., Clark, D. B., Rooney, G. G., Essery, R. L. H., Ménard, C. B., Edwards,
4 J. M., Hendry, M. A., Porson, A., Gedney, N., Mercado, L. M., Sitch, S., Blyth, E., Boucher,
5 O., Cox, P. M., Grimmond, C. S. B., and Harding, R. J.: The Joint UK Land Environment
6 Simulator (JULES), model description – Part 1: Energy and water fluxes, *Geosci. Model*
7 *Dev.*, 4, 677–699, doi:10.5194/gmd-4-677-2011, 2011

8 Bodas-Salcedo, A., Williams, K. D., Ringer, M. A., Beau, I., Cole, J. N. S., Dufresne, J.-L.,
9 Koshiro, T., Stevens, B., Wang, Z. and Yokohata, T.: Origins of the solar radiation biases
10 over the Southern Ocean in CFMIP2 models, *J. Climate*, 27, 41-56, doi:10.1175/JCLI-D-13-
11 00169.1., 2014.

12 Bodas-Salcedo, A., Hill, P. G., Furtado, K., Karmalkar, A., Williams, K. D., Field, P. R.,
13 Manners, J. C., Hyder, P. and Kato, S.: Large contribution of supercooled liquid clouds to the
14 solar radiation budget of the Southern Ocean, *J. Climate*, in press.

15 Bryan, F. O., Tomas, R., Dennis, J. M., Chelton, D. B., Loeb N. G. and McClean J. L.:
16 Frontal scale air-sea interaction in high-resolution coupled climate models, *J. Clim.*,
17 doi:10.1175/2010JCLI3665.1, 2010.

18 Cerovecki, I., Talley, L. D., Mazloff, M. R.: A Comparison of Southern Ocean Air-Sea
19 Buoyancy Flux from an Ocean State Estimate with Five Other Products. *Journal of Climate*.
20 24:6283-6306, 2011.

21 Chelton, D. B. and Xie, S.-P.: Coupled ocean-atmosphere interaction at oceanic mesoscales,
22 *Oceanography*, 23(4), 52-69, 2010.

23 Chelton, D. B., Schlax, M. G. and Samelson, R. M.: Global observations of nonlinear
24 mesoscale eddies, *Prog. Oceanogr.*, 91, 167-216, 2011.

25 Cunningham, S. A., Alderson, S. G., King, B. A. and Brandon, M. A.: Transport and
26 variability of the Antarctic Circumpolar Current in Drake Passage, *J. Geophys. Res.*, 108,
27 doi:10.1029/2001JC001147, 2003.

28 Delworth, T. L., Rosati, A., Anderson, W. G., Adcroft, A., Balaji, V., Benson, R., Dixon, K.
29 W., Griffies, S. M., Lee, H.-C., Pacanowski, R. C., Vecchi, G. A., Wittenberg, A. T., Zeng,

1 F., and Zhang, R.: Simulated climate and climate change in the GFDL CM2.5 high-resolution
2 coupled climate model. *Journal of Climate*, 25(8), doi:10.1175/JCLI-D-11-00316.1, 2012.

3 Deshayes, J., Treguier, A. -M., Barnier, B., Lecointre, A., Le Sommer, J., Molines, J.-M.,
4 Penduff, T., Bourdalle-Badie, R., Drillet, Y., Garric, G., Benshila, R., Madec, G., Biastoch,
5 A., Boening, C. W., Scheinert, M., Coward, A. C. and Hirschi, J. J.: Oceanic hindcast
6 simulations at high resolution suggest that the Atlantic MOC is bistable, *Geophys. Res. Lett.*,
7 40, 3069-3073 doi:10.1002/grl.50534, 2013.

8 Dickson R.R., Brown J.: The production of North Atlantic Deep Water: Sources, rates, and
9 pathways. *J Geophys Res* 99(C6):12,319–12,341, DOI 10.1029/94jc00530, 1994.

10 Eade, R., Smith D., Scaife A., Wallace E., Dunstone N., Hermanson L. and Robinson N.: Do
11 seasonal to decadal predictions underestimate the predictability of the real world?, *GRL*, DOI:
12 10.1002/2014GL061146, 2014.

13 ESMF: Earth System Modelling Framework Reference Manual for Fortran, 2014. Available
14 from
15 http://www.earthsystemmodeling.org/esmf_releases/public/ESMF_6_3_0rp1/ESMF_refdoc

16 Frenger, I., Gruber, N., Knutti, R. and Munnich, M.: Imprint of Southern Ocean eddies on
17 winds, clouds and rainfall, *Nature Geoscience*, 6, 608-612, 2013.

18 Ganachaud, A. and Wunsch, C.: Large-scale ocean heat and freshwater transports during
19 World Ocean Circulation Experiment, *J. Climate*, 16, 696-705, 2003.

20 Gordon C., Cooper, C., Senior, C. A., Banks, H., Gregory, J. M., Johns, T. C., Mitchell, J.
21 F. B., and Wood, R. A.: The simulation of SST, sea ice extents and ocean heat transports in a
22 version of the Hadley Centre coupled model without flux adjustments, *Climate Dynamics*, 16,
23 147-168, 2000.

24 Griffies, S. M., Winton, M., Anderson, W. G., Benson, R., Delworth, T. L., Dufour, C. O.,
25 Dunne, J. P., Goddard, P., Morrison, A. K., Rosati, A., Wittenberg, A. T., Yin, J. J. and
26 Zhang, R.: Impacts on Ocean Heat from Transient Mesoscale Eddies in a Hierarchy of
27 Climate Models, *J. Climate*, 28, 952-977, 2015.

28 Hall, M. M., and Bryden, H. L.: Direct estimates and mechanisms of ocean heat transport,”
29 *Deep-Sea Res.*, **29**, No. 3A, 339–359, 1982.

1 Hallberg, R.: Using a Resolution Function to Regulate Parameterizations of Oceanic
2 Mesoscale Eddy Effects. *Ocean Modelling*, 72, DOI:10.1016/j.ocemod.2013.08.007, 2013.

3 Hallberg, R.: Numerical insabilities of the ice/ocean coupled system. *CLIVAR Exchanges*,
4 65, 38-42, 2014.

5 Hewitt, H. T., Copsey, D., Culverwell, I. D., Harris, C. M., Hill, R. S. R., Keen, A. B.,
6 McLaren, A. J. and Hunke, E. C.: Design and implementation of the infrastructure of
7 HadGEM3: the next-generation Met Office climate modelling system, *Geosci. Model Dev.*, 4,
8 223-253, doi:10.5194/gmd-4-223-2011, 2011.

9 Hirabara, M., Tsujino, H., Nakano, H. And Yamanaka, G.: Formation mechanisms of the
10 Weddell Sea Polynya and the impact on the global abyssal ocean, *J. Oceanography*, 68 (5),
11 doi:10.1007/s10872-012-0139-3, 2012.

12 Hunke, E. C. and Lipscomb, W. H.: CICE: the Los Alamos sea ice model documentation and
13 software users' manual, Version 4.1, LA-CC-06-012, Los Alamos National Laboratory, N.M.,
14 2010.

15 Hunke, E. C., Lipscomb, W. H., Turner, A. K., Jeffery, N. and Elliott, S.: CICE: The Los
16 Alamos Sea Ice Model, Documentation and Software User's Manual, Version 5.1. Tech. Rep.
17 LA-CC-06-012, Los Alamos National Laboratory, Los Alamos, New Mexico. Available
18 from: <http://oceans11.lanl.gov/trac/CICE>, 2015.

19 Hurlburt, H. E., Brassington, G. B., Drillet, Y., Kamachi, M., Benkiran, M., Bourdalle-Badie,
20 R., Chassignet, E. P., Jacobs, G. A., Le Galloudec, O., Lellouche, J. M., Metzger, E. J.,
21 Smedstad, O. M., and Wallcraft, A. J.: High-Resolution Global and Basin-Scale Ocean
22 Analyses and Forecasts, *Oceanography*, 22(3), 110-127, 2009.

23 Ingleby, B. and Huddleston, M.: Quality control of ocean temperature and salinity profiles -
24 Historical and real-time data. *J. Mar. Sys.*, 65, 158-175, 2007.

25 Jones, D. C., Ito, T. and Lovenduski, N. S.: The transient response of the Southern Ocean
26 pycnocline to changing winds, *Geophys. Res. Lett.*, 38, L15604, doi:10.1029/2011GL048145,
27 2011.

28 Jones P. W.: A User's Guide for SCRIP: A Spherical Remapping and Interpolation Package,
29 Version 1.5, Los Alamos National Laboratory, 1998.

1 Jochumsen, K., Quadfasel, D., Valdimarsson, H. and Jonsson, S.: Variability of the Denmark
2 Strait overflow: Moored timeseries from 1996-2011, *J. Geophys. Res.*, 117, C12003,
3 doi:10.1029/2012JC008244, 2012.

4 Johns, T. C., Durman, C. F., Banks, H. T., Roberts, M. J., McLaren, A. J., Ridley, J. K.,
5 Senior, C. A., Williams, K. D., Jones, A., Rickard, G. J., Cusack, S., Ingram, W. J., Crucifix,
6 M., Sexton, D. M. H., Joshi, M. M., Dong, B. W., Spencer, H., Hill, R. S. R., Gregory, J. M.,
7 Keen, A. B., Pardaens, A. K., Lowe, J. A., Boda-Saloedo, A., Stark, S. and Searl, Y.: The new
8 Hadley Centre climate model HadGEM1: Evaluation of coupled simulations in comparison to
9 previous models, *J. Climate*, 19 (7), 1327–1353 , 2006.

10 McClean, J. L., Bader, D. C., Bryan, F. O., Maltrud, M. E., Dennis, J. M., Mirin, A. A., Jones,
11 P. W., Kim, Y. Y., Ivanova, D. P., Vertenstein, M., Boyle, J. S., Jacob, R. L., Norton, N.,
12 Craig, A. and Worley, P. H.: A prototype two-decade fully-coupled fine-resolution CCSM
13 simulation. *Ocean Modelling*, 39:10-30. 10.1016/j.ocemod.2011.02.011, 2011.

14 Macrander, A., Send, U., Valdimarsson, H., Jonsson, S. and Kase, R. H.: Interannual changes
15 in the overflow from the Nordic Seas into the Atlantic Ocean through Denmark Strait.
16 *Geophys Res Lett* 32(6):L06,606+, DOI 10.1029/2004gl021463, 2005.

17 Madec, G.: "NEMO ocean engine". Note du Pôle de modélisation, Institut Pierre-Simon
18 Laplace (IPSL), France, No 27 ISSN No 1288-1619, 2014.

19 Marzocchi, A., Hirschi, J. J. M., Holliday, N. P., Cunningham, S. A., Blaker, A. T. and
20 Coward, A. C.: The North Atlantic subpolar circulation in an eddy-resolving global ocean
21 model. *Journal of Marine Systems*, 142, 126-143. 10.1016/j.jmarsys.2014.10.007, 2015.

22 Megann, A.P., Storkey, D., Aksenov, Y., Alderson, S., Calvert, D., Graham, T., Hyder, P.,
23 Siddorn, J. and Sinha, B.: GO 5.0: The joint NERC-Met Office NEMO global ocean model
24 for use in coupled and forced applications. *Geosci. Model Dev.*, 7 (3). 1069-1092.
25 10.5194/gmd-7-1069-2014, 2014.

26 Meredith, M.P., Woodworth, P. L., Chereskin, T. K., Marshall, D. P., Allison, L. C., Bigg, G.
27 R., Donohue, K., Heywood, K. J., Hughes, C. W., Hibbert, A., Hogg, A. McC., Johnson, H.
28 L., Jullion, L., King, B. A., Leach, H., Lenn, Y.-D., Morales Maqueda, M. A., Munday, D. R.,
29 Naveira Garabato, A. C., Provost, C., Sallee J.-B., and Sprintall, J.: Sustained monitoring of
30 the Southern Ocean at Drake Passage: past achievements and future priorities. *Reviews of*
31 *Geophysics*, 49, RG4005, doi:10.1029/2010RG000348, 2011.

- 1 Minobe, S., Kuwano-Yoshida, A., Komori, N., Xie, S.-P. and Small, R. J.: Influence of the
2 Gulf Stream on the troposphere, *Nature*, 452, doi:10.1038/nature06690, 2008.
- 3 Mizielinski, M. S., Roberts, M. J., Vidale, P. L., Schiemann, R., Demory, M.-E., Strachan, J.,
4 Edwards, T., Stephens, A., Lawrence, B. N., Pritchard, M., Chiu, P., Iwi, A., Churchill, J., del
5 Cano Novales, C., Kettleborough, J., Roseblade, W., Selwood, P., Foster, M., Glover, M., and
6 Malcolm, A.: High-resolution global climate modelling: the UPSCALE project, a large-
7 simulation campaign, *Geosci. Model Dev.*, 7, 1629-1640, doi:10.5194/gmd-7-1629-2014,
8 2014.
- 9 Munday, D. R., Johnson, H. L. and Marshall, D. P.: Eddy saturation of equilibrated
10 circumpolar currents, *J. Phys. Oceanogr.*, 43, 507-532, 2013.
- 11 Palmer, M. D., and McNeall, D. J.: Internal variability of Earth's energy budget as simulated
12 by CMIP5 climate models, *Env. Res. Lett.*, 9 (3), 2014.
- 13 Pardaens A. K., Banks, H. T., Gregory, J. M. and Rowntree, P. R.: Freshwater transports in
14 HadCM3, *Climate Dynamics*, 21, 177-195, 2003.
- 15 Pradal, M.-A., and Gnanadesikan, A.: How Does the Redi Parameter for Mesoscale Mixing
16 Impact Global Climate in an Earth System Model? *Journal of Advances in Modeling the*
17 *Earth System*, 6:586-601, 2014.
- 18 Rae, J. G. L., Hewitt, H. T., Keen, A. B., Ridley, J. K., West, A. E., Harris, C. M., Hunke, E.
19 C. and Walters, D. N.: Development of Global Sea Ice 6.0 CICE configuration for the Met
20 Office Global Coupled Model, *Geosci. Model Dev.*, 8, 2221-2230, doi:10.5194/gmd-8-2221-
21 2015, 2015.
- 22 Sanchez-Gomez, E., Cassou, C., Ruprich-Robert, Y., Fernandez, E., and Teray, L.: Drift
23 dynamics in a coupled model initialized for decadal forecasts, doi :10.1007/s00382-015-2678-
24 y, *Clim. Dyn.*, 46, 1819–1840, 2016.
- 25 Sheldon, L., and Czaja, A.: Seasonal and interannual variability of an index of deep
26 atmospheric convection over western boundary currents. *Q J R Meteorol Soc* 140: 22–30. doi:
27 10.1002/qj.2103, 2014.
- 28 Small, R. J., Bacmeister, J., Bailey, D. A., Baker, A., Bishop, S., Bryan, F. O., Caron, J.,

1 Dennis, J., Gent, P. R., Hsu, H.-M., Jochum, M., Lawrence, D. M., Munoz Acevedo, E.,
2 diNezio, P., Scheitlin, T., Tomas, R., Tribbia, J., Tseng, Y. and Vertenstein, M.: A new
3 synoptic-scale resolving global climate simulation using the Community Earth System Model.
4 *Journal of Advances in Modeling Earth Systems*, 6, 1065-1094, DOI:
5 10.1002/2014MS000363, 2014.

6 Tréguier, A.-M., Deshayes, J., Lique, C., Dussin, R. and Molines, J.-M.: Eddy contributions
7 to the meridional transport of salt in the North Atlantic. *Journal of Geophysical Research.*
8 *Oceans*, Wiley-Blackwell, 117, doi:10.1029/2012JC007927, 2012.

9 Valcke, S., Craig, T. and Coquart, L.: OASIS3-MCT User Guide, OASIS3-MCT 3.0,
10 Technical Report, TR/CMGC/15/38, CERFACS/CNRS SUC URA No 1875, Toulouse,
11 France, 2015.

12 Vellinga, M. and Wu, P.: Low-Latitude Freshwater Influence on Centennial Variability of the
13 Atlantic Thermohaline Circulation. *J. Climate*, 17, 4498–4511, doi: 10.1175/3219.1, 2004.

14 Waters, J., Lea, D. J., Martin, M. J., Mirouze, I., Weaver, A. and While, J.: Implementing a
15 variational data assimilation system in an operational 1/4 degree global ocean model. *Q.J.R.*
16 *Meteorol. Soc.*, 141: 333-349. doi: 10.1002/qj.2388, 2015.

17 Weaver, A. T., Tshimanga, J. and Piacentini, A. : Correlation operators based on an implicitly
18 formulated diffusion equation solved with the Chebyshev iteration. *Q.J.R. Meteorol. Soc.*,
19 142: 455–471. doi: 10.1002/qj.2664, 2016.

20 Williams, K. D., Harris, C. M., Bodas-Salcedo, A., Camp, J., Comer, R. E., Copsey, D.,
21 Fereday, D., Graham, T., Hill, R., Hinton, T., Hyder, P., Ineson, S., Masato, G., Milton, S. F.,
22 Roberts, M. J., Rowell, D. P., Sanchez, C., Shelly, A., Sinha, B., Walters, D. N., West, A.,
23 Woollings, T. and Xavier, P. K.: The Met Office Global Coupled model 2.0 (GC2)
24 configuration. *Geosci. Model Dev.*, 8, 1509-1524, doi:10.5194/gmd-8-1509-2015, 2015.

25 Zhang Y. and Vallis, G. K.: Ocean Heat Uptake in Eddying and Non-Eddying Ocean
26 Circulation Models in a Warming Climate, *J. Phys. Oceanogr.*, 43 (10), 2211-2229,
27 doi:10.1175/JPO-D-12-078.1, 2013.

28

1 Table 1. Coupled models used in this paper

Model	Horizontal Resolution	Coupling frequency
GC2 (Williams et al., 2015)	N216-ORCA025	3-hourly
GC2-N512	N512-ORCA025	3-hourly
GC2.1 (this paper)	N216-ORCA025	1-hourly
GC2.1-N512O12	N512-ORCA12	1-hourly

2

3

4 Table 2. Key metrics from years 11-20 of the experiments and observations. TOA
 5 observations from CERES/EBAF for years 2000-2010. Global mean SST error (compared to
 6 Reynolds OI). Overflows are calculated as southward flow across the Greenland-Iceland-
 7 Scotland ridge below density of 27.8 kg m^{-3} and have standard deviation shown in brackets.

Model	Net TOA (W/m^2)	Global mean SST error (K)	Maximum overturning at 30°S (Sv)	Maximum overturning at 24°N (Sv)	Net transport from overflows (Sv)
Observations	0.85				
GC2	1.61	0.25	13.7	14.6	4.0 (0.24)
GC2-N512	1.79	0.60	14.3	14.9	3.9 (0.28)
GC2.1	1.64	0.29	14.3	16.4	4.7 (0.26)
GC2.1- N512O12	2.02	0.44	17.5	17.7	5.9 (0.42)

8

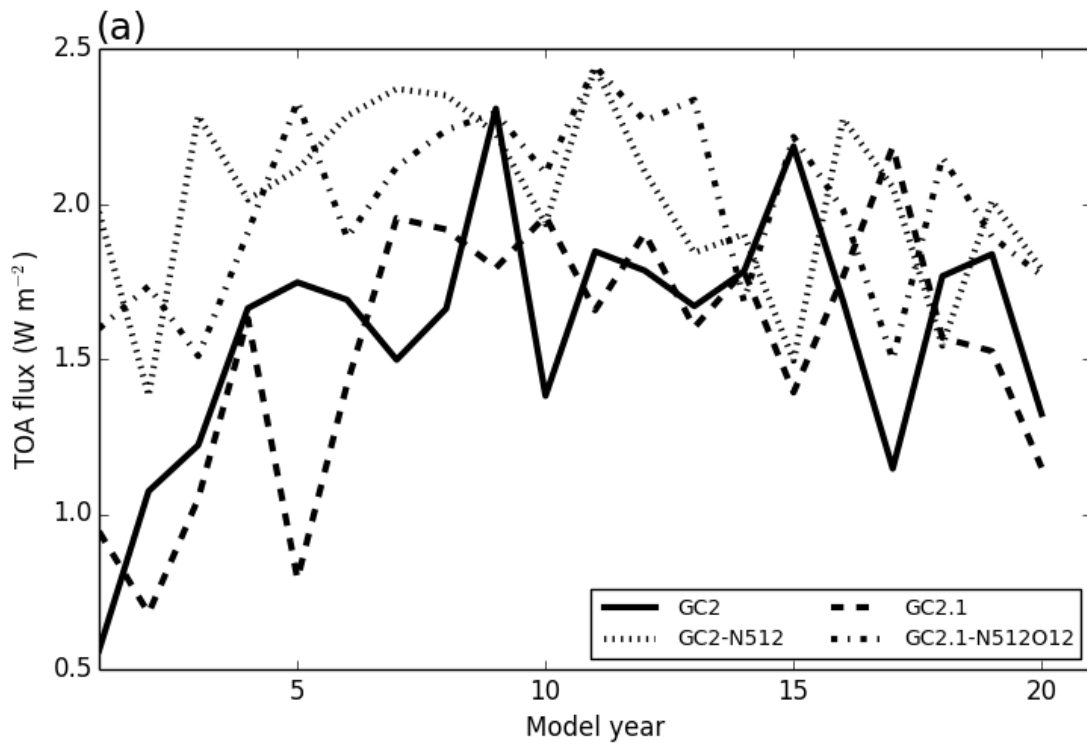
9

10

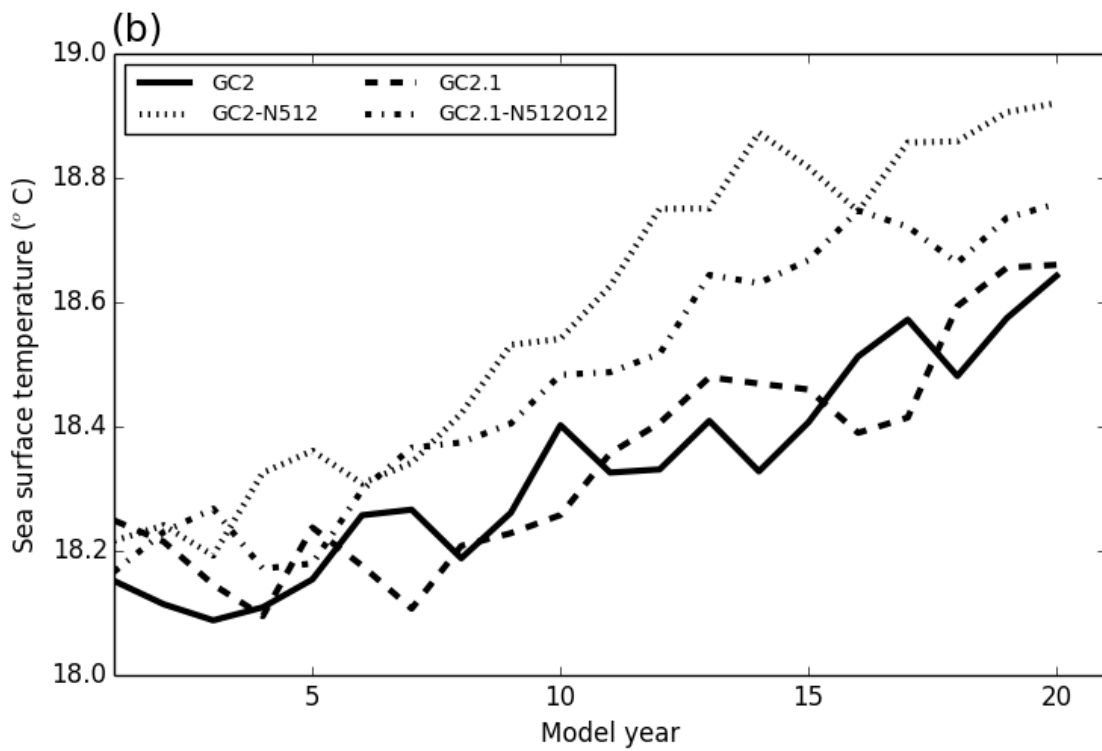
11

12

13



1

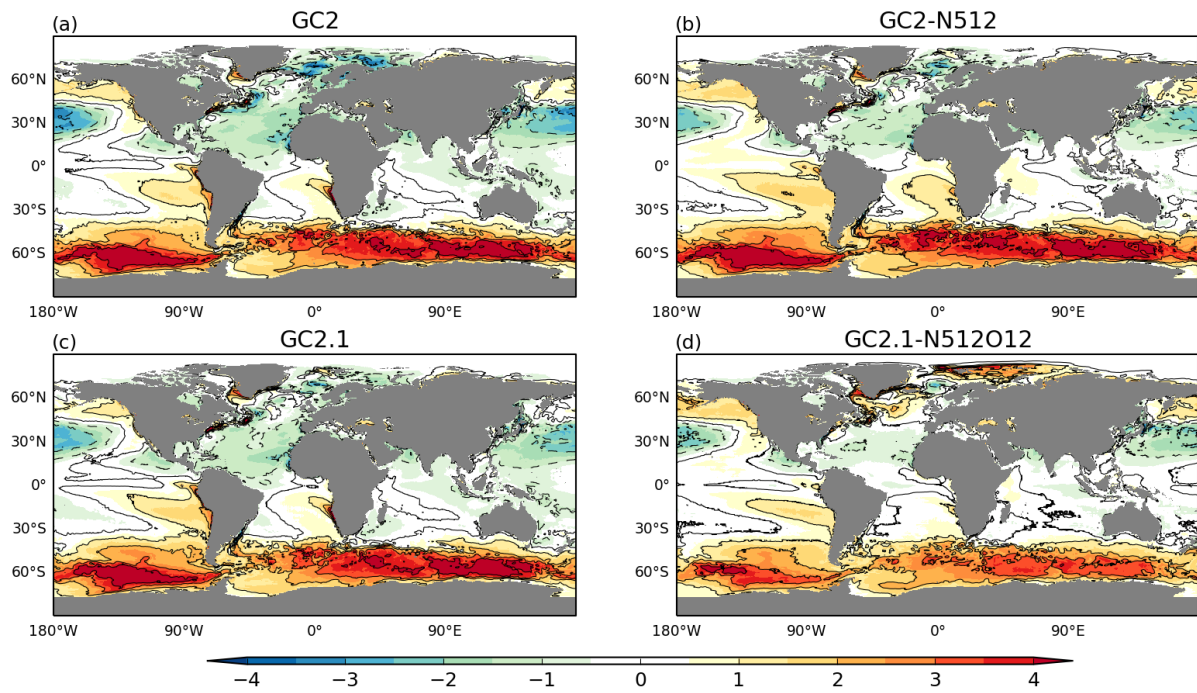


2

3 Figure 1: Timeseries of a) net TOA and b) global mean SST from GC2, GC2-N512, GC2.1
 4 and GC2.1-N512O12.

5

6

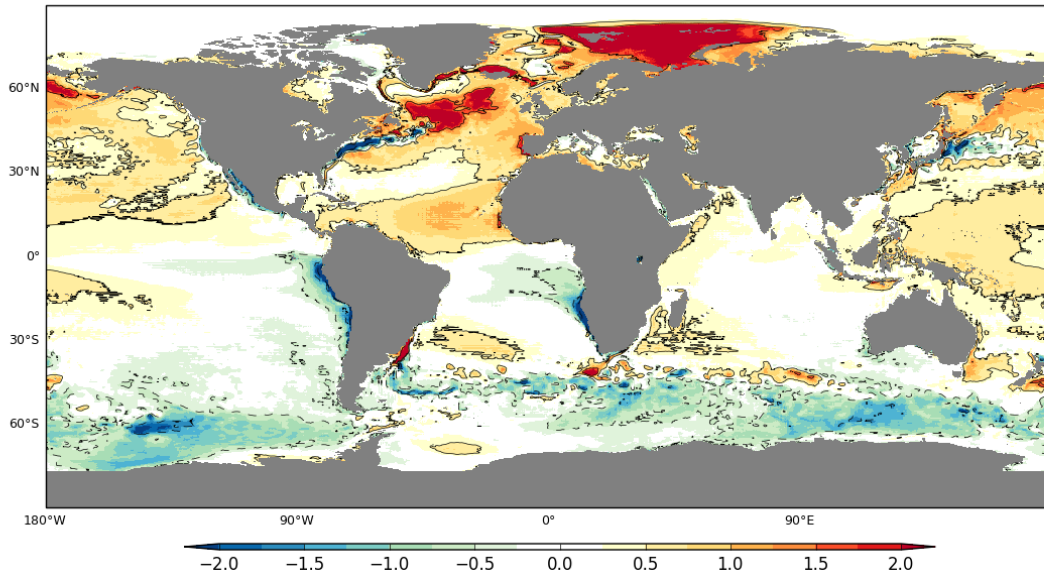


1

2 Figure 2: Differences between modelled SST from years 11-20 and observed SST from
 3 HadISST (°C) for a) GC2, b) GC2-N512, c) GC2.1 and d) GC2.1-N512O12.

4

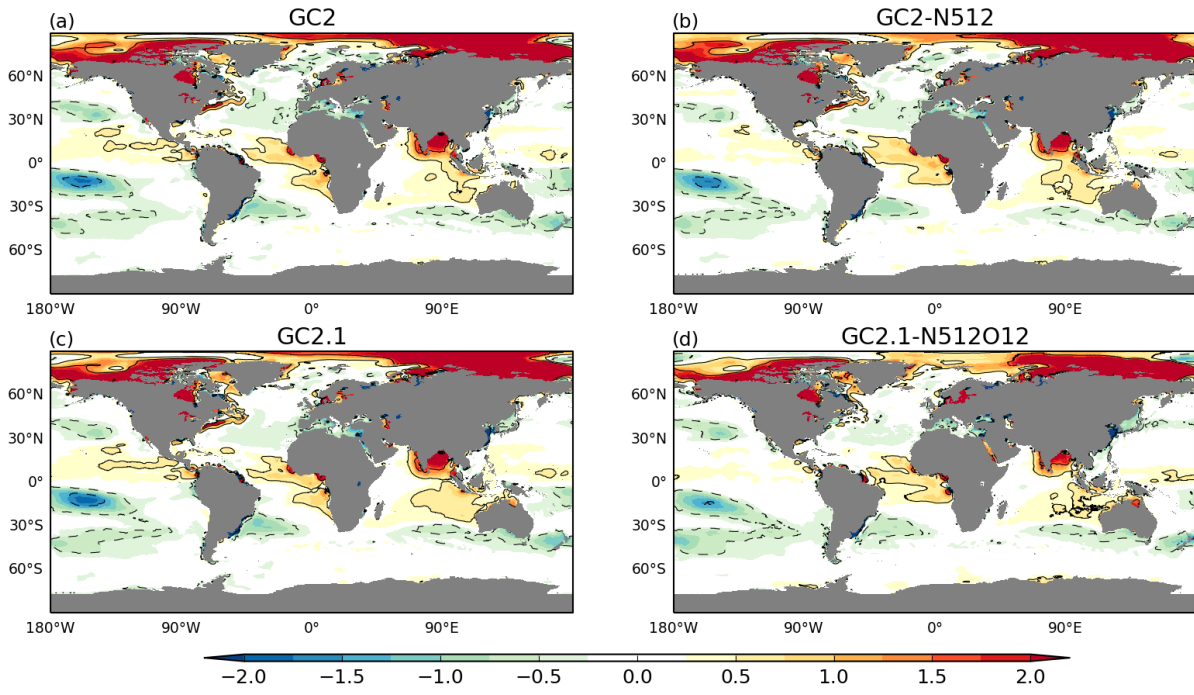
5



1
2
3

Figure 3: SST difference (°C) for years 11-20 between GC2.1-N512O12 and GC2.1

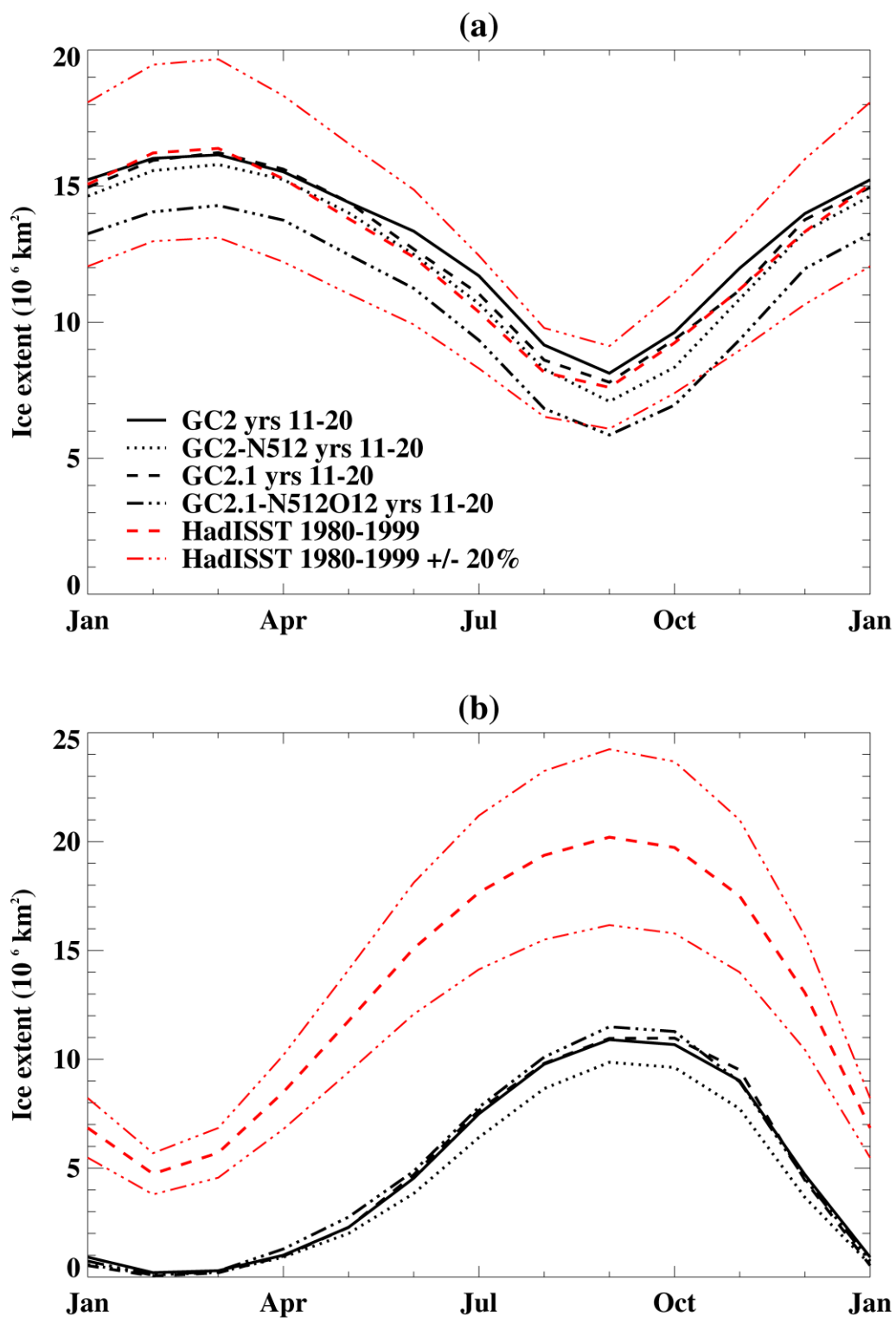
1



2
3

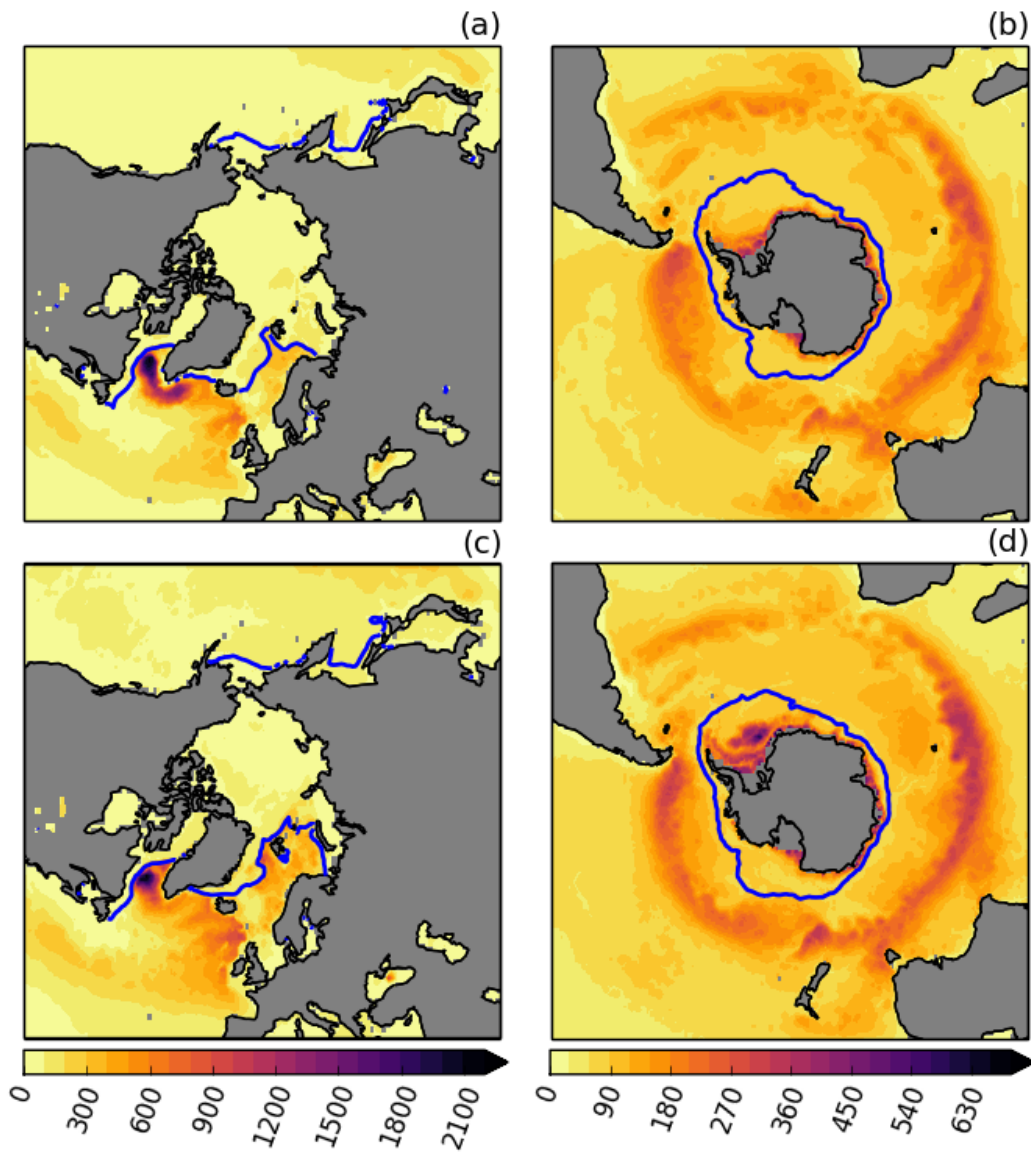
4 Figure 4: Differences between modelled SSS from years 11-20 and observed SSS from EN4
5 (psu) for a) GC2, b) GC2-N512, c) GC2.1 and d) GC2.1-N512O12.

6



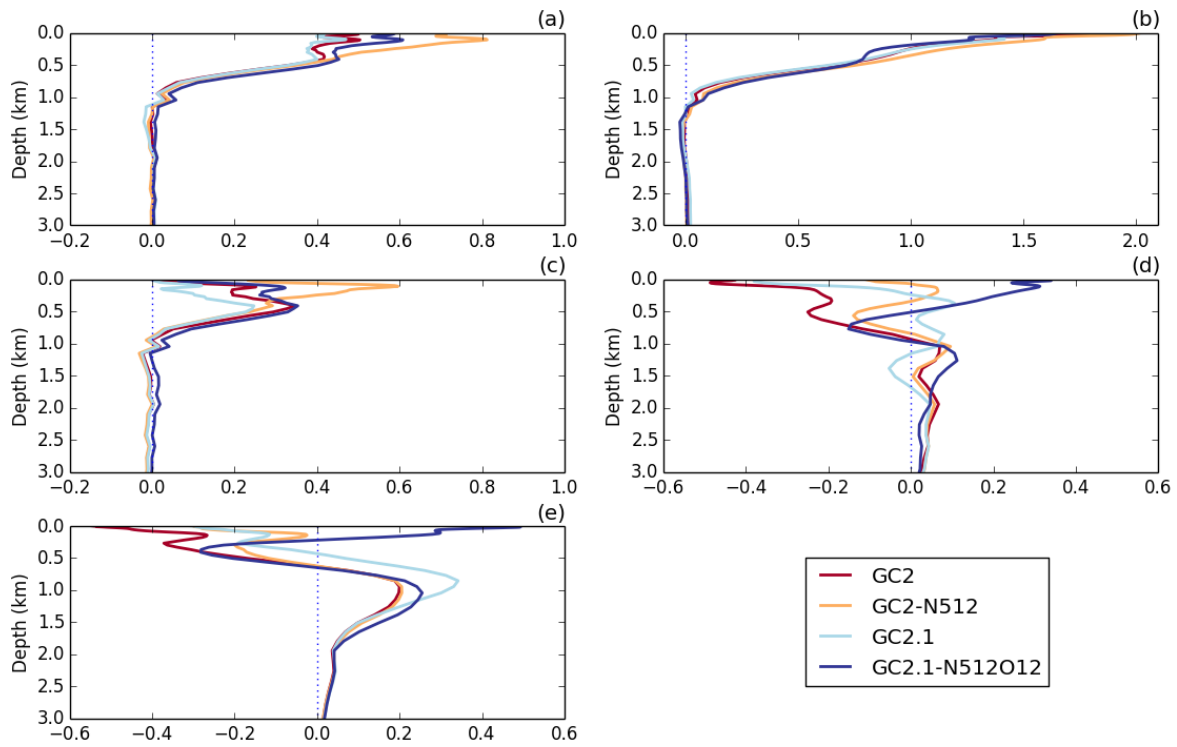
1
2
3
4
5

Figure 5: Seasonal cycle of sea ice extent in a) Northern and b) Southern hemisphere for years 11-20 compared against HadISST 1980-99 and with +/- 20% error bars denoted.



2
3
4
5
6
7
8
9

Figure 6: Mean March Northern hemisphere winter mixed layer depth (m) and sea ice edge and mean September Southern hemisphere winter mixed layer depth (m) and sea ice edge for years 11-20 for GC2 (a,b) and GC2.1-N512O12 (c,d). The sea ice edge (marked in blue) is based on a threshold of 15% ice concentration.



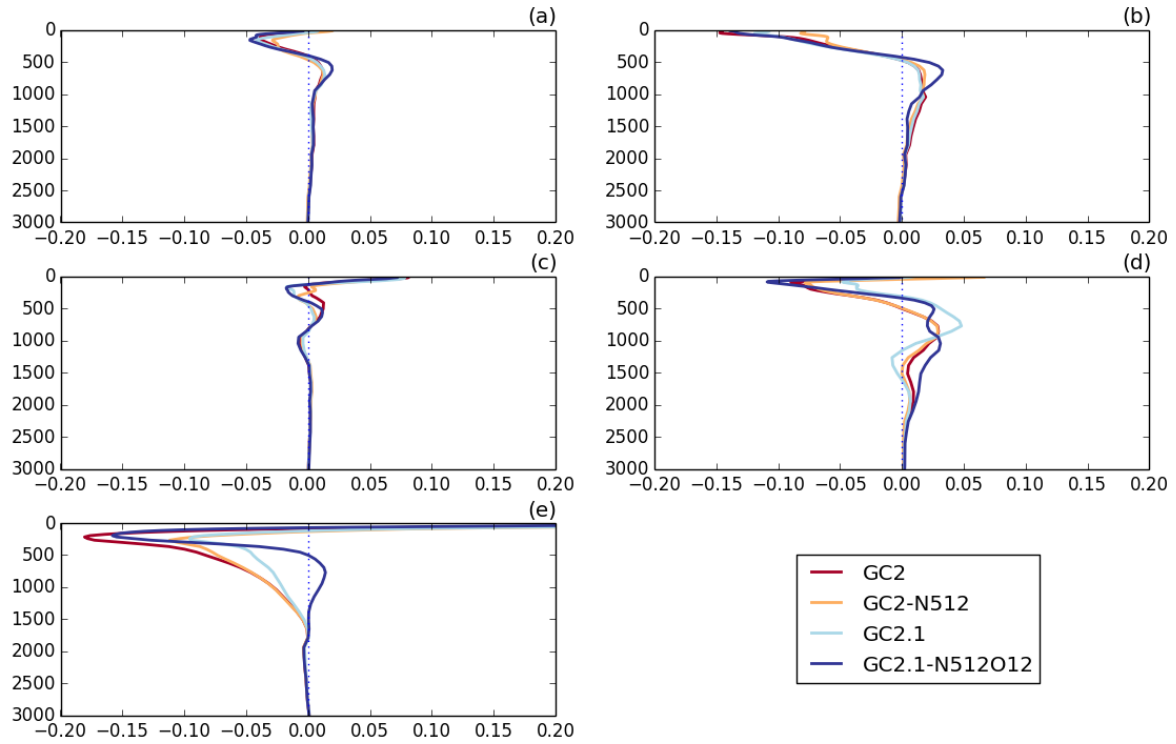
1

2

3 Figure 7: Area-weighted mean temperature difference (years 11-20 minus year 1; °C) for
 4 GC2, GC2-N512, GC2.1 and GC2.1-N512O12 for a) global, b) 90S-30S, c) 30S-30N, d)
 5 30N-90N, e) 65N-90N. Note the range on the x-axis is equal in all panels except (b). The
 6 vertical axis denotes depth (m).

7

8

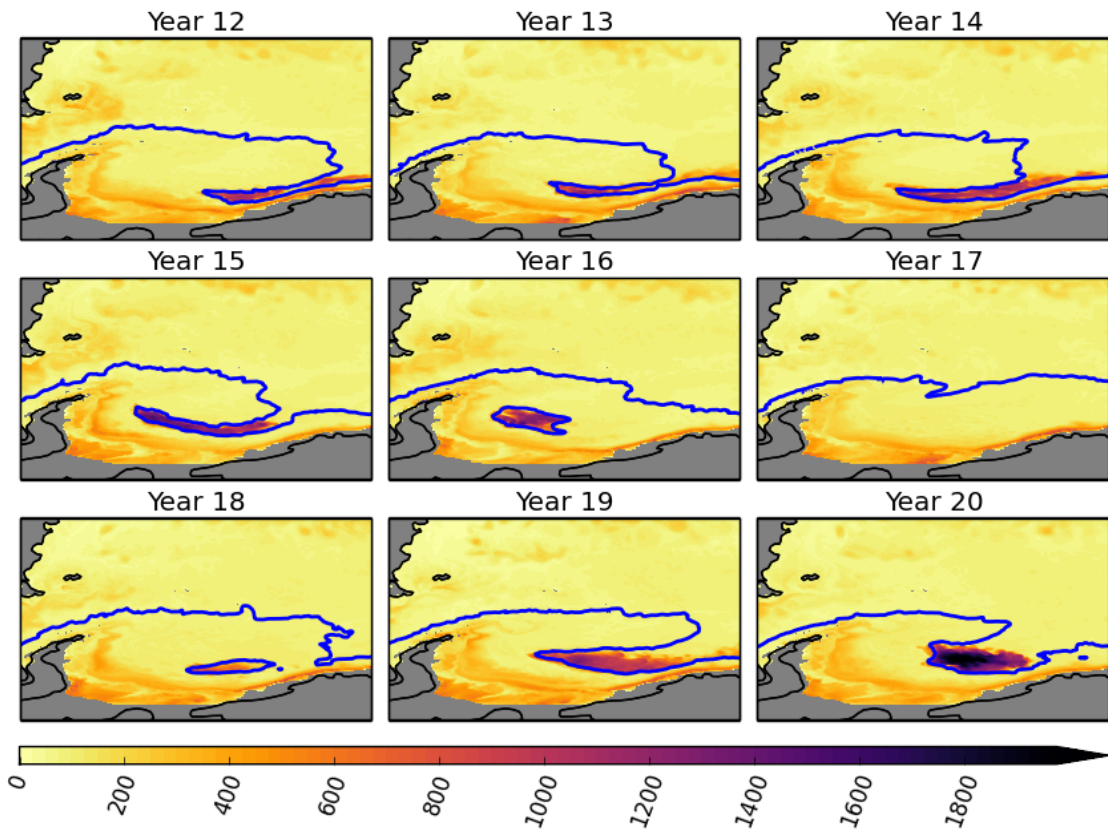


1

2 Figure 8: Area-weighted mean salinity difference (years 11-20 minus year 1; psu) for GC2,
 3 GC2-N512, GC2.1 and GC2.1-N512O12 for a) global, b) 90S-30S, c) 30S-30N, d) 30N-90N,
 4 e) 65N-90N. The vertical axis denotes depth (m).

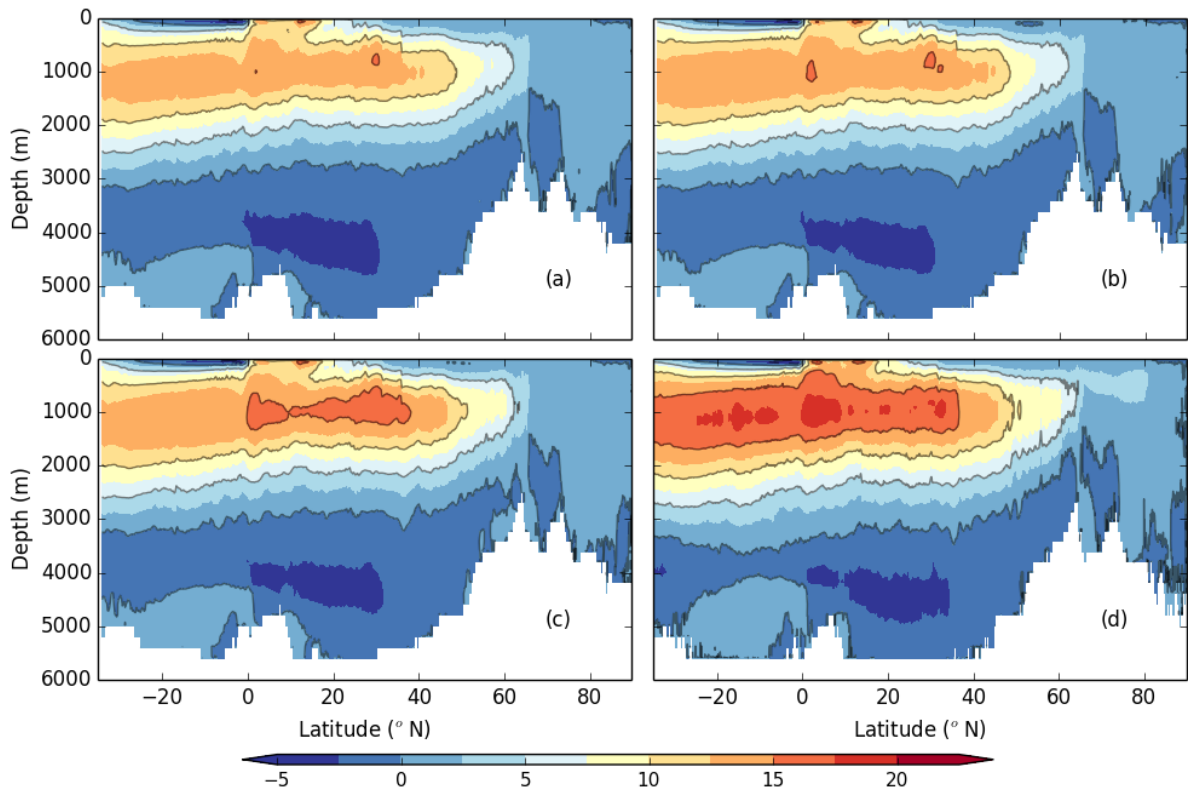
5

6



1
2
3
4
5
6
7

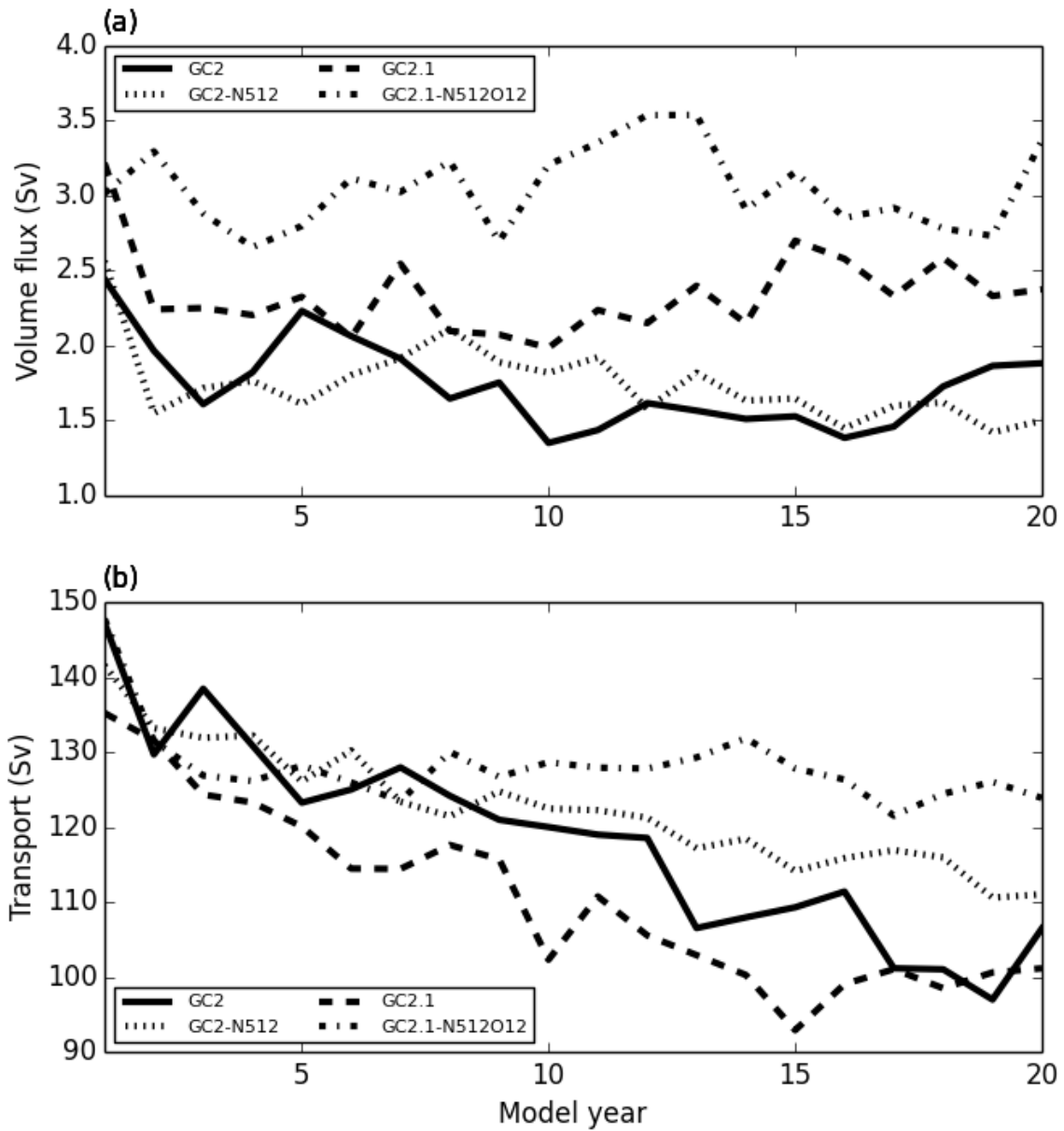
Figure 9: September mixed layer depth (m) and sea ice edge in GC2.1-N512O12 for years 12-20 indicating the presence of a Weddell Sea polynya. The sea ice edge (marked in blue) is based on a threshold of 15% ice concentration.



1
2
3
4
5
6
7
8
9

Figure 10: Atlantic Meridional overturning for (a) GC2, (b) GC2-N512, (c) GC2.1 and (d) GC2.1-N512O12, meaned over years 11-20. Contours in Sverdrups ($10^6 \text{ m}^3 \text{ s}^{-1}$), with line contour spacing of 5 Sv.

1

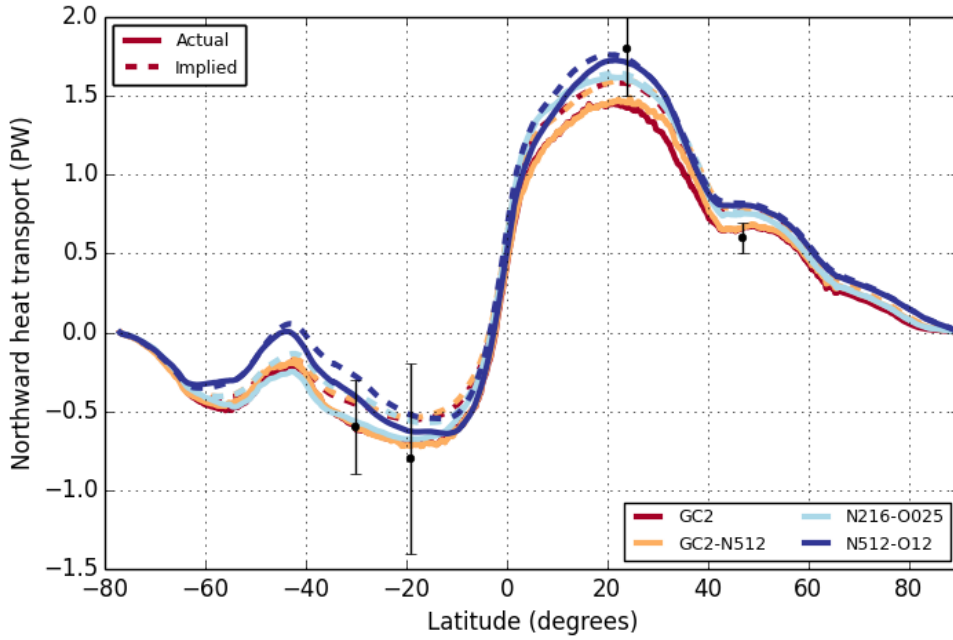


2

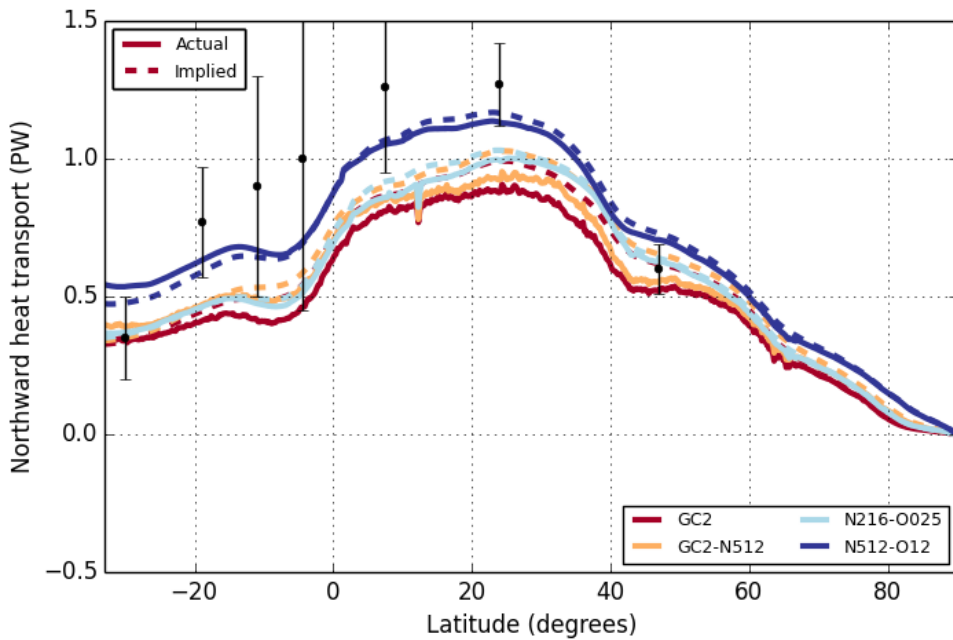
3

4 Figure 11: a) Denmark Straits volume flux (Sv) (calculated as southward flow across the
5 Greenland-Iceland-Scotland ridge below density of 27.8 kg m^{-3}) and b) Antarctic Circumpolar
6 Current transport (Sv) from GC2, GC2-N512, GC2.1 and GC2.1-N512O12

7



1
2



3

4 Figure 12: Actual (bold) and implied (dashed) northward heat transports from GC2, GC2-
 5 N512, GC2.1 and GC2.1-N512O12 for (a) global and (b) Atlantic basins. The implied
 6 transport (integrated southwards from the North Pole using the ocean surface heat flux) uses
 7 heat fluxes in which the global mean imbalance has been removed at every point.
 8 Observational estimates and associated error bars from Ganachaud and Wunsch (2003) are
 9 shown.